https://doi.org/10.33805/2639-6734.105
Volume 1 • Issue 1 | Page 1 of 6

EDELWEISS PUBLICATIONS
OPEN ACCESS

Journal of Heterocyclics

Research Article

ISSN: 2639-6734

Synthesis and Characterization of Te Doped ZnO Nanosheets For Photocatalytic Application

N Shanmugam*, S Suthakaran, N Kannadasan, K Sathish kumar

Abstract

In this paper, we report the synthesis of tellurium (Te) doped ZnO nanocrystals for photocatalytic applications. X-ray diffraction, Fourier transforms infrared, photoluminescence and field emission scanning electron microscope are the techniques employed to characterize the properties of the prepared products. The photocatalytic activities of the undoped and doped ZnO are analyzed by the degradation of brilliant green (BG). The results of the degradation reveal that ZnO doped with Te has higher photocatalytic performance than undoped ZnO.

Key words: diffraction, photoluminescence, degradation, brilliant green, photocatalytic

Introduction

In the modern scientific era the materials in the nanoscale have gained more attention than their bulk form owing to their peculiar physical and chemical properties [1]. In the semiconductor industry nanocrystalline ZnO has many applications for numerous fields, such as lasers, sensors, solar cells and field emission devices due to its higher band gap and larger excitation binding energy (60 MeV). Among the organic pollutants, brilliant green (BG) creates an impact on its enriched outreaching to the environment through effluent of textiles and paint industries [2-9]. Brilliant green can create so many toxic effects on the human beings and animals; therefore its degradation needs more attention. As a result of nontoxic nature and low coast, ZnO is an alternate to TiO_2 in the degradation of organic pollutants [10-12]. Doping that does essential incorporation of ions of particular elements into the host material to tailor its properties is a widely accepted technique in the semiconductor industry. Further, the morphology control through doping is another major task as the size and shape can influence various properties of the prepared products. Doping ZnO with tellurium (Te) can tailor the luminescence properties of ZnO by passivation of oxygen defects. Already few works are available on the Te doped ZnO film [13-16]. Previously we have studied the photocatalytic properties of ZnO on cerium doping [17]. In the present work, we have attempted to tailor the photocatalytic properties of ZnO by incorporating Te in the lattices of Zn^{2+}. For that tellurium in different proportions (0.1, 0.15, 0.2, and 0.25 M) are doped into ZnO through a simple chemical precipitation method. The prepared products are analysed for their structural, optical, morphological, and photocatalytic properties.

Materials and Methods

All the chemicals used in this study are of AR grade with 99% purity (E.Merck) and used without further purification. Sample preparation and dilutions were made of ultrapure water. Zinc nitrate hydrate [$Zn(NO)_3.6H_2O$], sodium telluride [Na_2Te] and potassium hydroxide (KOH) were used as precursors.

For the synthesis of Te-doped ZnO, 7.4 g (0.5 M) of zinc nitrate hydrate dissolved in 50 ml of deionized water was stirred vigorously by magnetic stirrer and sodium telluride of preferred mole (0.1, 0.15, 0.2, and 0.25 M) prepared in 20 ml aqueous was mixed drop wise. Then, 6.2 g (2.5 M) of potassium hydroxide in 50 ml of deionized water was added drop by drop to the above mixture. The entire was stirred magnetically at 60 °C until a white precipitate was formed. The obtained dispersions were purified

Affiliation:
Department of Physics, Annamalai University, Chidambaram 608 002, Tamilnadu, India

***Corresponding author:**
Department of Physics, Annamalai University, Chidambaram 608 002, Tamilnadu, India.
Tel: +91-9444276357
E-mail: quantumgosh@rediffmail.com.

Citation: Shanmugam N, Suthakaran S, Kannadasan N, Sathishkumar K (2015) Synthesis and Characterization of Te Doped ZnO Nanosheets For Photocatalytic Application. J O Heterocyclics 105: 15-20

Received: August 12, 2015
Accepted: September 19, 2015
Published: September 26, 2015

Copyright: © 2015 Shanmugam N. This is an open-access article distributed under the terms of the Creative Commons Attribution License, which permits unrestricted use, distribution, and reproduction in any medium, provided the original author and source are credited.

by dialysis against de-ionized water and ethanol several times to remove impurities. The purified products were dried in hot air oven at 100 °C for 6 h to evaporate water and organic materials to the maximum extent. The dried powders were pulverized to fine powders using agate mortar for further characterizations. A similar method of preparation without the addition of tellurium was used to synthesize undoped ZnO Nano crystals.

For the purpose of studying the photocatlytic activity of ZnO, 0.2 g of ZnO was added to a quartz photoreactor containing 100 ml of a 1 mg/l brilliant green (BG) aqueous solution. After stirring for 120 min in the dark in order to reach the absorption equilibrium, the mixture was irradiated with sunlight with intensity fluctuation of 950 ± 25 Wm^{-2}. The residual BG in the aqueous solution was analyzed by checking the absorbance at 624 nm in the UV-Vis absorption spectra. To determine the percentage of degradation of MB, the samples were collected at regular intervals (for every 30 min), filtered and centrifuged to remove the nanophotocatalyst particles that exist as undissolved particles in the sample and studied using UV-Vis absorption. The degradation percentage of the dye in the presence and absence of ZnO nanopartices can be calculated from the following equation [18].

$$\% D = \frac{C_0 - C_t}{C_0} \times 100 \quad (1)$$

Where C_0 is the initial concentration of the dye and C_t is the concentration of dye after irradiation in selected time interval. The same procedure was adopted for tellurium doped ZnO nanoparticles.

The crystalline phase and particle size of pure and Te-doped ZnO nanoparticles were analyzed by X-ray diffraction (XRD) measurement which was carried out at room temperature by using X'PERT-PRO diffractometer system (scan step of 0.05° (2θ), counting time of 10.16s per data point) equipped with a Cu tube for generating Cu Kα radiation (k = 1.5406 Å); as an incident beam in the 2-theta mode over the range of 10°–80°, operated at 40 kV and 30 mA. The photoluminescence (PL) emission spectra of the samples were recorded with a Spectroflurometer (Jobin Yvon, FLUOROLOG–FL3-11). The functional groups were determined by SHIMADZU-8400 Fourier-transform infrared spectrometer in which the IR spectra were recorded by diluting the milled powders in KBr and in the wavelength between 4000 and 400 cm^{-1} was used to assess the presence of functional groups in pure and Te-doped ZnO. The morphological analysis was performed by HITACHI S-4700 field emission scanning electron microscope (FESEM). Energy-dispersive spectrum (EDS) analysis of the products was performed during FESEM measurements. The UV-Visible absorption measurements of the products during photocatalytic measurements were recorded in the wavelength range of 350-750 nm using Shimadzu UV1800 spectrophotometer.

Results and Discussion

In Figure 1 (a), we show the XRD patterns of pure and different proportions of tellurium (0.1, 0.15, 0.2 and 0.25 M) doped ZnO nanocrystals. As seen in the figure, the entire patterns exhibit only the peaks corresponding to the ZnO wurtzite structure with preferred orientation along (101) direction. However, no peaks related to tellurium and other complex oxides are seen, revealing the purity of the synthesized products. Figure 1 (b) shows the enlarged regional XRD patterns of the sample within the 2θ angle of 30-38°. From the figure, it is clear that predominant peaks of ZnO are shifted to relatively lower 2θ values with an increase in Te concentration, suggesting successful doping of Te ions into the ZnO lattice. The potential shift to lower 2θ value is reasonable, as a lattice enlargement was expected due to the ionic radius difference between Te^{4+} (0.97 Å) and Zn^{2+} (0.74 Å) ions [19]. The lattice parameter variation with increasing Te amount was calculated and listed in Table 1. the change in the value of "c" from 5.202 Å for pure ZnO to 5.213 Å for highest amount of Te doping (0.025 M) clearly indicates the increase in the lattice size upon doping. The increase in the lattice parameters can be explained through two possible ways. The first one is due to replacement of Zn^{2+} and O^- ions by large ionic radius Te^{4+} ions compared with O^- and Zn^{2+}. The second possibility can be caused by interstial incorporation of Te^{4+} ions into the lattice. The c/a parameter which should be 1.633 for ideal hexagonal close packed structure has also been changed with Te doping, and is shown in Table 1. The crystallite sizes of the products were estimated using Scherre's formula

$$D = \frac{0.89\,\lambda}{\beta\, cos\, \theta} \quad (2)$$

Where, λ is the X-ray wavelength, θ is the Bragg's angle and β is the full width at half maximum. As shown in Table 1, the crystallite size of ZnO decreases with increasing content of Te up to 0.2 M and shows no change on 0.25 M of doping. Usually, particle growth

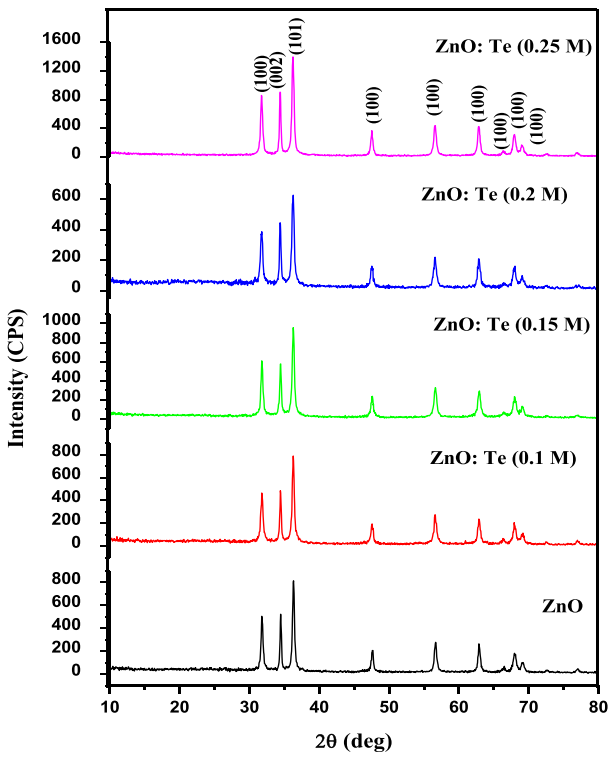

Figure 1A: X-ray diffraction patterns of ZnO and various levels of Te doped ZnO nanosheets.

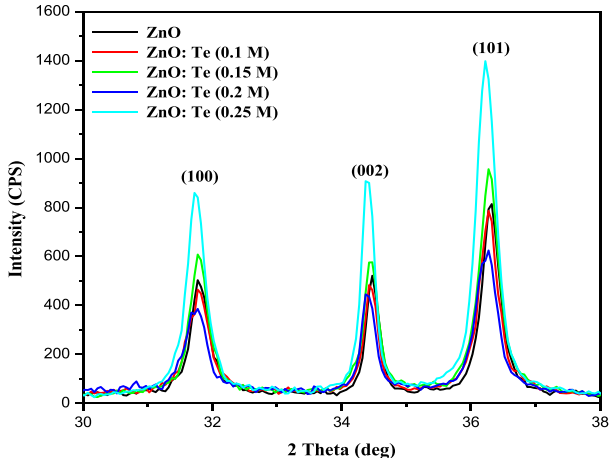

Figure 1B: X-ray diffraction patterns of ZnO and Te doped ZnO nanosheets enlarged view of (100), (002) and (101) peaks.

Samples	Particle size (nm)	Lattice parameters (Å)		
		a=b	c	c/a
ZnO	26	3.25	5.202	1.6
ZnO: Te (0.1 M)	25	3.253	5.209	1.601
ZnO: Te (0.2 M)	22	3.255	5.211	1.601
ZnO: Te (0.15 M)	21	3.249	5.206	1.602
ZnO: Te (0.25 M)	26	3.248	5.213	1.604

Table 1: XRD derived parameters of undoped and Te doped ZnO nanoparticles.

can be prevented by introducing constraints to the motion of the grain boundaries. In the present case, the incorporated Te ions generate a retarding force with high impact than the driving force responsible for grain growth. If the retarding force is more than the driving force for the grain growth, the particles cannot grow any longer. Therefore, the presence of Te ions in the ZnO prohibited the grain growth of the ZnO.

The change in the bond length of ZnO has been calculated from the following formula and the resulted are tabulated.

$$L = \sqrt{\left(\frac{a^2}{3} + \left(\frac{1}{2} - u\right) c^2\right)} \quad (3)$$

Where, the parameter u is giving by

$$u = \frac{a}{3c^2} + 0.25 \quad (4)$$

It has been seen that the bond length value of ZnO increases on low level of Te doping ($\leqq 0.15$ M) and decreases at higher doping concentrations (≥ 0.15 M).

The room temperature PL emission spectra of ZnO and ZnO: Te with 320 nm excitation are shown in Figure 2. All the samples exhibit an UV and four visible emissions. The obtained UV emission at 390 nm is attributed to the near band edge emission of ZnO, originating from the excitonic transitions between the electrons in the conduction bands and the holes in the valence bands [20]. The appearance of blue emission at 437 nm originates from zinc interstitial. The blue green emission centered at 487 nm is due to a radiative transition of an electron from the deep donal level of Zn_i to an acceptor level of neutral V_{zn} [21]. The intense red emission at 643 nm can be ascribed to oxygen-related defects [22]. Significantly, the defect related emissions of the host material can be tuned by dopant material. In the present case, the PL intensity of ZnO strongly depends on the concentration of Te. At the initial stage, in the absence of dopant, emission peaks have higher intensity, however, on increasing the concentration of doping the intensity reduction can be seen with the broadening of the FWHM as a function of Te content. This strongly suggests that the density of oxygen defects responsible for red emissions could be controlled by doping of Te in the host material ZnO. The same type of passivation of oxygen defects on Te doping was reported by other researcher [15].

To know the influence of Te doping on the Zn-O bonding, FT-IR spectra were recorded for undoped and doped ZnO in the range of 4000- 400 cm^{-1}. The obtained spectra are presented in Figure 3. The appearance of absorption peaks around 3414 and 1630 cm^{-1} can be ascribed to O-H stretching and bending vibrations, respectively [23]. The broad band absorbed around 2368 cm^{-1} can be related to the O = C = O vibration of CO_2 molecule exist in air [24]. The presence of nitrate peaks at around 883 cm^{-1} can be originated from zinc nitrate used as zinc source. The broad absorption feature positioned at 431 cm^{-1} is due to stretching vibration of Zn-O [25]. On doping, stretching vibrations of Zn-O are shifted to lower and higher energy regions as a result of change in bond length. Such a change in bond length of Zn-O already has been discussed in the XRD section.

The FESEM image of ZnO exhibits that the particles are having spherical morphology with homogeneous size distribution (Figure 4a). The corresponding histogram exhibits the average particle size as 23 nm (Figure 4b). The influence of Te doping on the morphology of ZnO is clearly seen from the Figure 4c. As shown in figure, the doped product is in the form of nanosheets stack together. These nano-sheets are showing regular hexagonal structure of thickness 27 nm (Figure 4d). The EDS analysis of Te doped ZnO (Figure 4e) reveals that Zn. O, and Te are the constituents of the prepared material.

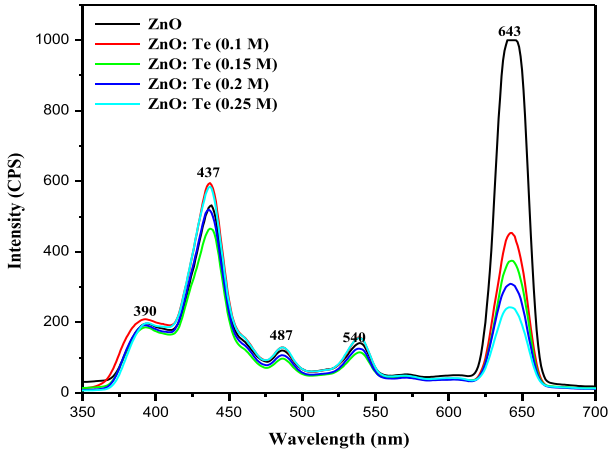

Figure 2: PL emission spectra of ZnO and various levels of Te doped ZnO nanosheets.

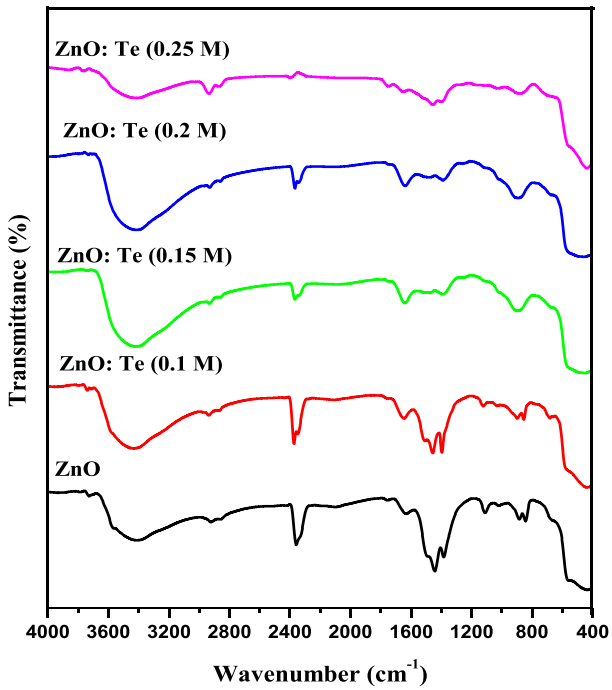

Figure 3: FT-IR spectra of ZnO and various levels of Te doped ZnO nanosheets.

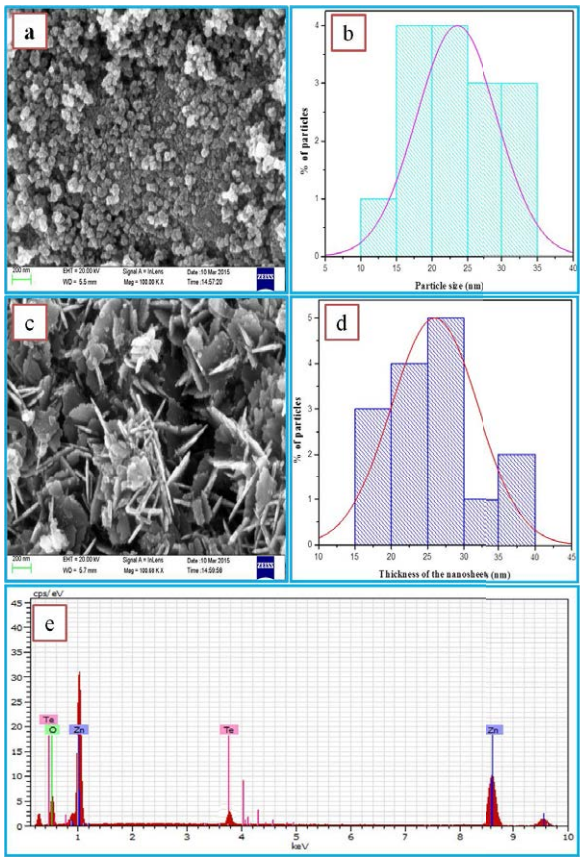

Figure 4: FESEM images of (a, b) ZnO, corresponding particle size distribution histograms (c, d) Te (0.2 M) doped ZnO nanosheets, corresponding thickness of the nanosheets distribution histograms and (c) corresponding EDX pattern.

In the evaluation of photo catalytic activity of ZnO and ZnO: Te against Brilliant green (BG), 100 ml of BG aqueous solution (1 mg/L) was taken in a quartz photo reactor. Further, 0.2 g of ZnO was added into the quartz photo reactor. Before irradiation, the reaction mixture was stirred in dark for 30 min to achieve the absorption- desorption equilibrium between the catalyst and dye molecules. The Sunlight with intensity fluctuation of 950 ± 25 wm^{-2} was used as an irradiation source. During the course of light irradiation, 5 ml of sample was collected at regular intervals (every15 min), filtered and centrifuged to remove the undissolved photocatalyst. The filtrate was analyzed by UV-Vis spectrometer at P_{max} = 624 nm and the photodegradations were calculated by equation (1).

The photocatalytic activity is based on the reactive nature of an electron-hole pair generated in the semiconductor nanoparticles. Under illumination by light of energy greater than the semiconductor band gap, electron is excited to the conduction band and electron in the conduction band migrates to the lattice surface. If no recombination takes place, these charge carriers can react with adsorbed molecules.

Figures 5(a) and 5(b) exhibit the change in absorbtion pattern of BG exposed to Sunlight for varies irradiation times in the presence of ZnO and ZnO: Te, respectively. The percentage of degradation was calculated using the equation 1 and the results are given in Table 2. From the table, it is clear that after 120 min of light irradiation, 75 % of dye was degraded in the presence of ZnO. However, for ZnO: Te, the degradation rate was increased to 86% at the same 120 min of light irradiation. This result revealed that Te doped ZnO exhibited higher photocatalytic activity than pure ZnO. Further, the rate constant values for dye degradation for the catalysts were calculated using the first order rate eqution [17].

$$\ln\frac{C_0}{C_t} = kt \qquad (5)$$

Where k is the first order rate constant, Figure 6 shows the plot depicting a linear relationship between $\ln\frac{C_0}{C_t}$ and time for all

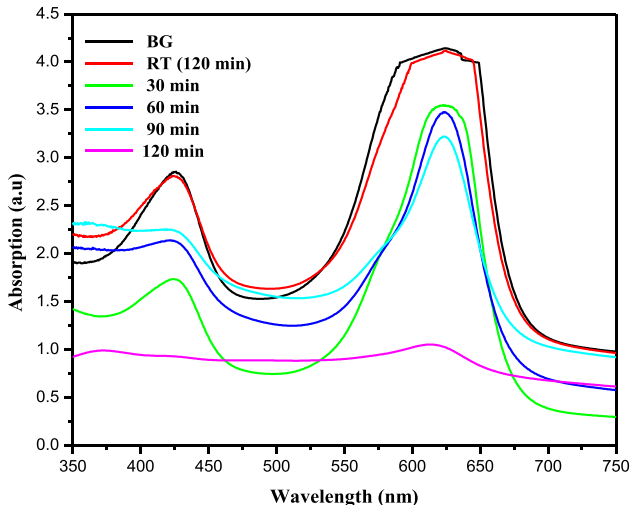

Figure 5A: Time dependent UV-Vis absorption spectra of the photocatalytic degradation of BG in the presence of ZnO nanoparticles.

Time	Degradation (%)	
	ZnO	ZnO: Te (0.2M)
DR (120 min)	1	7
30	14	13
60	16	15
90	22	64
120	75	86

Table 2: The effect of BG dye degradation by ZnO and Te (0.2 M) doped ZnO nanosheets.

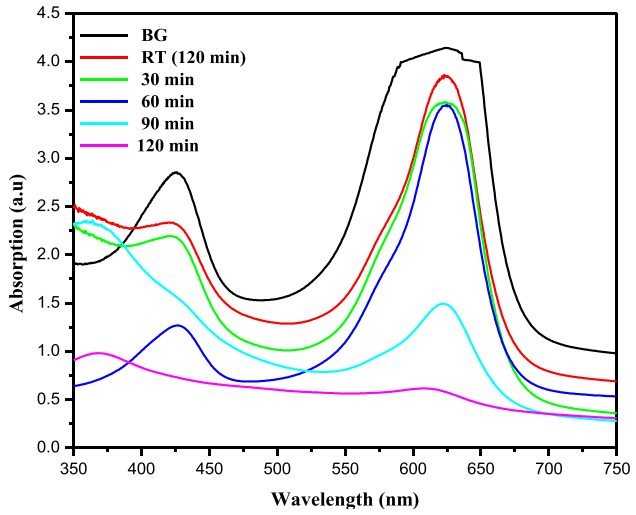

Figure 5B: Time dependent UV-Vis absorption spectra of the photocatalytic degradation of BG in the presence of tellurium (0.2 M) doped ZnO nanosheets.

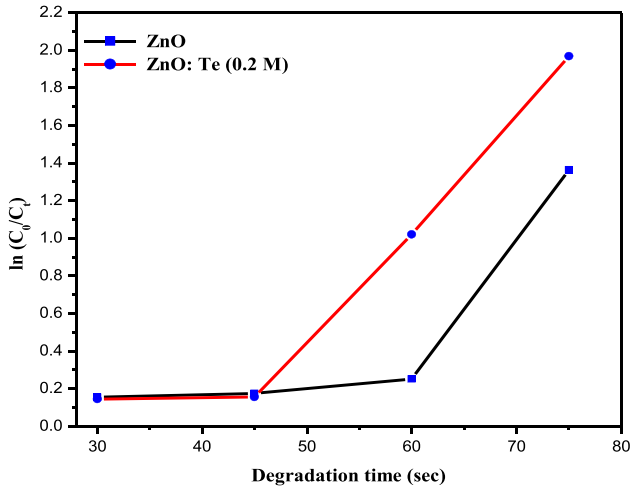

Figure 6: Kinetic study of photo degradation of BG in the presence of ZnO and tellurium (0.2 M) doped ZnO nanosheets.

the samples and from the slope of the graph, rate constant values were calculated. The value of rate constant for undoped ZnO was found to be 0.01235 min^{-1}, whereas, for ZnO: Te, it was increased to 0.02111 min^{-1}. The increased k value suggests the improved photocatalytic activity of ZnO on Te doping. The possible mechanism behind the improved photocatalytic activity of Te doped ZnO is explained as follows.

When light of energy greater than forbidden gap is irradiated, electrons from the valance band can make a quantum jump to conduction band of ZnO. The presence of dopant Te^{4+} within the crystal matrix or on the surface of ZnO can trap the photogenerated electrons or holes and subsequently transfer the same to adsorbed oxygen and hydroxyl ions to generate super oxide radicals ($O_2^{\cdot -}$) and hydroxide radicals ($^{\cdot}OH$), respectively. This behavior will reduce the electron-hole recombination and generates more and more free radicals responsible for the degradation of BG. In this way ZnO doped with Te reveals higher activity to the degradation of the dye brilliant green.

Conclusion

In summary, high quality nanocrystals of pure and Te doped ZnO have been synthesized through a simple chemical precipitation approach. The XRD patterns suggest the formation of wurtzite ZnO nanocrystals with a size of 24 nm. The sizes of the samples could be controlled up to the concentration of 0.2 M of tellurium and were found to be independent at 0.25 M of doping. The PL spectra of the doped products show the intensity quenched red emissions suggesting the passivation of oxygen defects. The change in the ZnO bond length on doping has been confirmed by FT-IR analysis. The FESEM analysis of the products reveals a change in morphology of ZnO from spherical particles to nanosheets on Te doping. The EDS pattern of Te-doped ZnO exhibits the presence of Zn, O, and Te as expected. The doping of Te showed an enhancement of the photocatalytic activity of ZnO against brilliant green (BG). The enhanced photocatalytic activity of Te doped ZnO suggesting its usage as a scavenger against the pollutant brilliant green which is being discharged from the textiles industries.

References

1. SN Das, JP Kar, JH Choi, TI Lee, KJ Moon, et al. Fabrication and characterization of ZnO single nanowire-based hydrogen sensor (2010) Journal of Physical Chemistry C 114:1689.
2. Huang MH, Mao S, Feick H, Yan H, Wu Y, et al. Room-temperature ultraviolet nanowire nanolasers (2001) Science 292:1897-1899.
3. DM Bagnall, YF Chen, Z Zhu, T Yao, S Koyama, et al. Optically pumped lasing of ZnO at room temperature (1997) Appl Phys Lett 70:2230-2232.
4. ZS Wang, CH Huang, YY Huang, YJ Hou, PH Xie, et al. A highly efficient solar cell made from a dye-modified ZnO-covered TiO2 nanoporous electrode (2001) Chem Mater 13:678.
5. Z Liu, C Liu, J Ya, E Lei. Controlled synthesis of ZnO and TiO2 nanotubes by chemical method and their application in dye-sensitized solar cells (2011) Renew. Energy 36:1177.
6. CJ Lee, TJ Lee, SC Lyu, Y Zhang, H Ruh, et al. Field emission from well-aligned zinc oxide nanowires grown at low temperature (2002) Appl. Phys. Lett 81:3648.
7. Law M, Greene LE, Johnson JC, Saykally R, Yang P. Nanowire dye-sensitized solar cells (2005) Nat Mater 4:455-459.
8. D Sridevi, KV Rajendran. Synthesis and optical characteristics of ZnO nanocrystals (2009) Bull. Mater. Sci 32:165.
9. Goldberger J, Sirbuly DJ, Law M, Yang P. ZnO nanowire transistors (2005) J Phys Chem B 109:9-14.
10. YH Jang, ST Kochuveedu, MA Cha, YJ Jang, JY Lee, et al. Synthesis and Photocatalytic Properties of Hierarchical Metal Nanoparticles/ZnO Thin Films Hetero Nanostructures Assisted by Diblock Copolymer Inverse Micellar Nanotemplates (2010) J. Colloid Interface Sci. 345:125-130.

11. M Wu, B Yang, Y Lv, Z Fu, J Xu, et al. Efficient one-pot Synthesis of Ag Nanoparticles Loaded on N-Doped Multiphase TiO2 Hollow Nanorod Arrays With Enhanced Photocatalytic Activity (2010) Appl. Surf. Sci, 256:7125-7130.

12. MR Hoffmann, ST Martin, W Choi, DW Bahnemann. Environmental Applications of Semiconductor Photocatalysis (1995) Chem. Rev 95:69-96.

13. Savas Sönmezoglu, Erdi Akman. Improvement of physical properties of ZnO thin films by tellurium doping (2014) Applied Surface Science 318:319-323.

14. A Iribarren, P Fernández, J Piqueras. Recombination processes in Te-doped ZnO microstructures (2013) Phys. Status Solidi B:1–6.

15. Farid Jamali Sheini, Ramin Yousefi, MR Mahmoudian, Nabeel Ali Bakr, Abdolhossein Sa, et al. Facile synthesis of different morphologies of Te-doped ZnO nanostructures (2014) Ceramics International 40:7737-7743.

16. A Iribarren, P Ferna´ndez, J Piqueras. Cathodoluminescence study of Te-doped ZnO microstructures grown by a vapour–solid process (2008) J Mater Sci 43:2844–2848.

17. N Kannadasan, N Shanmugam, S Cholan, K Sathishkumar, G Viruthagiri,et al. The effect of Ce4+ incorporation on structural, morphological and photocatalytic characters of ZnO nanoparticles (2014) Materials Characterization 97:37-46.

18. Pouretedal HR, Norozi A, Keshavarz MH, Semnani A. Nanoparticles of zinc sulfide doped with manganese, nickel and copper as nanophotocatalyst in the degradation of organic dyes (2009) J Hazard Mater 162:674-681.

19. K Sathishkumar, N Shanmugam. N Kannadasan, S Cholan, G Viruthagiri. Influence of Zn2+ ions incorporation on the magnetic and pseudo capacitance behaviours of NiO nanoparticles (2014) Material Science in Semiconductor Processing 27:846-853.

20. N Kannadasan, N Shanmugam, S Cholan, K Sathishkumar, R Poonguzhali,et al. Synergistic effect of bimetal ions (Ce, Pb) incorporation on optical, structural, and sensory activity of ZnO nanocrystals (2014) J Solid State Electrochem 3:757-768.

21. Gunjan Srinet, Ravindra Kumar, Vivek Sajal. Structural, optical, vibrational, and magnetic properties of sol-gel derived Ni doped ZnO nanoparticles (2013) Journal of Applied Physics 114:033912.

22. OL Stroyuk, VM Dzhagan, VV Shvalagin, SY Kuchmiy. Size-Dependent Optical Properties of Colloidal ZnO Nanoparticles Charged by Photoexcitation (2010) J. Phys. Chem. C 114:220.

23. K Sathishkumar, N Shanmugam, N Kannadasan, S Cholan, G Viruthagiri. Opto, magnetic and electrochemical characterization of Ni1-xCoxO nanocrystals (2014) J. Mater Sci: Mater Electron 3:1881-1889.

24. Shi L, Gunasekaran S. Preparation of Pectin-ZnO Nanocomposite (2008) Nanoscale Res Lett 3: 491-495.

25. N Kannadasan, N Shanmugam, K Sathishkumar, S Cholan, G Viruthagiri, et al. Optical behavior and sensor activity of Pb ions incorporated ZnO nanocrystals (2015) spectrochimica Acta Part A: Molecular and Biomolecular spectroscopy 143:179-186.